Bioactive Materials 34 (2024) 298–310

Contents lists available at ScienceDirect

Bioactive Materials

journal homepage: www.keaipublishing.com/en/journals/bioactive-materials

A bioactive composite hydrogel dressing that promotes healing of both acute and chronic diabetic skin wounds

Shunlai Shang [a,b], Kaiting Zhuang [b], Jianwen Chen [b], Ming Zhang [c], Shimin Jiang [a,**], Wenge Li [a,*]

[a] Department of Nephrology, China-Japan Friendship Hospital, Beijing, China
[b] Department of Nephrology, First Medical Center of Chinese PLA General Hospital, Nephrology Institute of the Chinese People's Liberation Army, National Key Laboratory of Kidney Diseases, National Clinical Research Center for Kidney Diseases, Beijing Key Laboratory of Kidney Disease Research, Beijing, 100853, China
[c] Department of Nephrology, Affiliated Beijing Chaoyang Hospital of Capital Medical University, Beijing, 100020, China

ARTICLE INFO

Keywords:
Exosomes
Bioactive glass
Diabetic wound
Anti-inflammatory
Titanium dioxide

ABSTRACT

Mesenchymal stem cell derived exosomes (MSC-Exos) demonstrate beneficial effects on wound healing via anti-inflammatory and angiogenic properties. Chitosan (CS) exhibits excellent biocompatibility and accelerates cellular migration, adhesion, and proliferation. The ions released from bioactive glass (BG) and titanium dioxide (TiO_2) nanoparticles exhibit sustained angiogenic and antibacterial potency. In this study, CMCS-CEBT hydrogel was synthesized from exosomes encapsulated carboxymethyl chitosan (CMCS), chitosan nanoparticles (CS-NPs), BG, and TiO_2 nanoparticles for a preliminary evaluation of its impacts on the treatment of full-thickness skin defects, diabetic wounds, and burn skin injury due to burns. In vitro analysis indicated that the hydrogel exhibits excellent cell compatibility, stimulates endothelial cell adhesion and proliferation, and presents anti-inflammatory, angiogenic, and antibacterial activities. In vivo, the composite hydrogel dressing accelerated a wound healing acceleration effect, stimulated angiogenesis, and increased collagen deposition and the expression of anti-inflammatory factors. This innovative composite hydrogel dressing as a potential clinical therapy, utilizing bioactive materials, holds promise as a potential clinical therapy that aims to facilitate the regeneration of acute and chronically damaged skin tissue.

1. Introduction

The skin is the outermost layer of the body, and it functions to safeguard internal tissues against mechanical damage, limit water loss, and prevent the entry of pathogens. Moreover, it isolates UV radiation and regulates body temperature [1]. A variety of physical, chemical, and biological factors may compromise the skin's integrity and cause acute or chronic injuries or wounds. The skin wound healing process is crucial and intricate, involving multiple stages, including hemostasis, inflammation, cell proliferation, and tissue regeneration to repair damaged tissues, restore functionality, and heal the affected area. However, wound trauma remains a significant clinical concern worldwide, due to the long-term morbidity associated with tissue repair and regeneration, bleeding, infection risk, as well as sepsis, and scar hypertrophy and formation [2]. A prolonged wound healing time is primarily caused by chronic inflammation, reduced production of growth factors, persistent microbial infection, and impaired angiogenesis [3]. Reduced proliferation, migration, and transposition of primitive cells, such as fibroblasts and keratinocytes, are other critical factors that cause delayed healing and impede the formation of functional skin [4].

Wound dressings are important tools for promoting wound healing [5–7]. The ideal wound dressing should serve as a protective layer to cover the site exposed by skin damage, and it should have sufficient mechanical properties, moisture retention, exudate absorption, and haemostasis, excellent antibacterial activity, anti-inflammatory activity, and promoting of angiogenesis and granulation tissue regeneration to promote promoting the healing process. The ideal wound dressing should also have good biocompatibility, biodegradability, and water

Peer review under responsibility of KeAi Communications Co., Ltd.
* Corresponding author.
** Corresponding author.
E-mail addresses: 18810568600@163.com (S. Shang), 2719059128@qq.com (K. Zhuang), ilwincjw2015@126.com (J. Chen), cyyyzm@139.com (M. Zhang), minjiang101@163.com (S. Jiang), wenge_lee2002@126.com (W. Li).

https://doi.org/10.1016/j.bioactmat.2023.12.026
Received 22 November 2023; Received in revised form 28 December 2023; Accepted 29 December 2023

absorption and retention, and no cytotoxicity.

Substantial progress has been made regarding the utilization of hydrogel materials in various biomedical applications, given their ability to simulate the dynamic properties of the natural extracellular matrix (ECM) through their highly hydrated microenvironments. As nontraditional implantable and dynamic agents for tissue therapy, injectable hydrogels demonstrate immense potential. A viable approach to enhancing the functionality of these hydrogels in vivo is through the fabrication of multicomponent composite hydrogels to achieve diverse functions within the intricate networks of the hydrogels [8]. A wide array of both organic and inorganic fillers, including ceramic, carbon-based, metallic, and polymeric materials, have been integrated into hydrogel matrices to create composites with enhanced mechanical and biological traits, as well as adjustable functionalities [9]. Recently, the fusion of composite hydrogels with bioactive glass (BG), which is characterized by its biological potency, biocompatibility, angiogenic capabilities, and osteogenic effects, has attracted considerable scientific attention.

Stem cells can be used to effectively treat both acute and chronic wounds effectively due to their potent secretory function [10,11]. Notably, stem cell-derived extracellular vesicles mediate wound repair processes via anti-inflammatory effects, stimulation of angiogenesis, and collagen deposition [12–14]. Combining extracellular vesicles with biologically active materials for sustained release results in better targeting and longer lasting therapeutic effects than intravenous infusion of extracellular vesicles. Nanotechnology is becoming an important tool in skin regenerative medicine [15,16]. Nanoscale components exhibit increased cell growth, migration, and differentiation compared to their counterparts. They simulate the dynamic environment in which cells must survive [17]. Wound healing nanomaterials fall into two categories: (1) beneficial nanomaterial systems; and (2) nanomaterial carriers of bioactive compounds. A variety of nanocarrier systems have been validated in vitro and have therapeutic potential but require further in vivo investigation. Combinations of nanoparticles and nanocarriers may yield synergistic outcomes, stimulating accelerated wound repair [18].

Chitosan has advantageous biological qualities such as biocompatibility, biodegradability, nontoxicity, outstanding swelling ability, mucosal adhesion ability, stability, anticancer activity, proinflammatory effects, coagulation -promoting effects, and wound-healing activity [19]. The positive surface charge of chitosan enables it to effectively support cell growth, promote surface-induced thrombus formation and blood coagulation, and accelerate in vivo coagulation by modulating platelet activation. Chitosan promotes homeostasis and occlusion by absorbing proteins and adhering to platelets. The amino groups of chitosan acquire H+ in acidic environments, carrying positive charges that can be used to capture extracellular vesicles [8,9]. In addition, chitosan has a sustained release effect on extracellular vesicles and is suitable as a carrier for wound healing [20].

BG therapy significantly increases epithelial cell proliferation, weakens the inflammatory response, and enhances angiogenesis [21]. BG, a multicomponent bioactive inorganic material capable of adopting various shapes (such as particles or fibers), represents an innovative wound dressing alternative. BG contains proangiogenic ions and demonstrates excellent stability, affordability, and clinical safety. Inorganic dressings increase heightened early angiogenesis and stimulate skin tissue formulation. Numerous studies have highlighted how BG induces improved superior soft tissue healing by stimulating repair mechanisms. This translates into improved conditions for skin healing [22].

Carboxymethyl chitosan (CMCS), a chitosan derivative obtained via carboxymethylation, offers excellent biocompatibility and a broad range of applications in gene therapy, drug delivery, and tissue engineering [23]. Employing sponge structures derived from CMCS, membranes, and hydrogel dressings exhibit ideal water permeability, breathability, and hemostatic capabilities. Currently, hydrogel treatments for both acute and chronic wounds are proving successful. This finding correlates with the strong physical similarities between hydrogel biomaterials and the natural extracellular matrix, which promote improved wound healing outcomes.

Using animal skin injury models and clinical trials, we found that improper treatment of skin trauma can cause great harm to human health. Full-thickness skin defects lead to various inflammation and infection, and wound bleeding. Diabetic wounds and ulcers that are difficult to heal are one of the most challenging complications in current clinical practice, and may even cause gangrene, amputation, etc [24]. Improper treatment of partial burns can cause serious complications such as sepsis, shock, kidney function problems and circulatory failure, and even death [25].

This study utilized chitosan to formulate nanoparticles capable of accumulating and capturing MSC-derived exosomes, which were encapsulated with CMCS hydrogels, and loaded with BG and titanium dioxide (TiO_2) to construct a hydrogel dressing composed of chitosan nanoparticles, MSC- derived, BG, and TiO_2 (CMCS-CEBT) for the treatment of deep skin lesions, diabetic wounds, and burns.

This study has certain value. Through the combination of organic and inorganic active substances, we prepared a composite hydrogel dressing aimed at regulating wound microecology and promoting rapid wound recovery. Our composite hydrogel dressing is unique in that it has multiple clinical uses in the treatment of three different types of skin injuries.

2. Reagents and methods

All experiments were approved by the China-Japan Friendship Hospital's Animal Research Ethics Committee approval (No.: zryhyy21-22-10-03).

2.1. Materials

Chitosan (deacetylation degree ≥95 %, 200–400 mPa s, Aladdin, China) was used. NaOH was purchased from Sigma-Aldrich. Experimental water was obtained from the Millipore Milli-Q ultrapure system. Alpha-MEM (Gibco, USA), foetal bovine serum (Gibco, USA), and penicillin-streptomycin solution (Gibco, USA) were used for cell culture. Carboxymethyl chitosan was obtained from Qingdao Biotemed Biomaterial Co., Ltd. Exosomes were isolated using the traditional ultracentrifugation (UC) method. BG was purchased from Beijing Daqing Biotechnology Co., Ltd. Alpha-MEM (Gibco, USA), foetal bovine serum (Gibco, USA) and 1 % penicillin-streptomycin solution (Gibco, USA) were used. CD31 antibodies (ab181595, Abcam, Cambridge, UK), α-SMA antibodies (BM0002, Boster, Wuhan, China).antibodies of TNF-α(17590-1-AP),IL-1β(26048-1-AP), IL-6 (21865-1-AP), IL-10 (60269-1-Ig), VEGFA (19003-1-AP), VEGFR2 (26415-1-AP) and GAPDH antibodies were purchased from Proteintech (Wuhan, China). Calnexin (ab22595, abcam, Britain), TSG101 (72312, CST, USA) CD63 (PAB48050, Bioswamp, China) and CD9 (13174, CST, USA) antibodies were used Animals. C57 mice and BD mice were provided by SPF (Beijing) Biotechnology Co., Ltd.

2.2. Production and characterization of chitosan nanoparticles

The process used to generate chitosan nanoparticles adhered to a previously reported protocol with minor adjustments. Initially, 1 % (v/v) acetic acid was incorporated into chitosan to yield a final concentration of 0.5 % (w/v). Subsequently, the pH was adjusted to 4.6–4.8 using 10 N NaOH. Then, 0.25 % tripolyphosphate was added to the solution at a ratio of 1:3 (tripolyphosphate: chitosan solution). Under a magnet, self-assembly of chitosan nanoparticles occurred easily. Purification involved centrifuging the nanoparticles at 9000×*g* for 30 min, discarding the supernatant, and then washing with water to eliminate sodium hydroxide residues. These steps allowed the reformation of chitosan nanoparticles in a 2 % (w/v) solution.

2.3. Extraction of exosomes

MSCs isolated from fresh human umbilical cords were prepared by digestion and centrifugation, as described previously. MSCs were cultured in α-MEM (Gibco, USA) containing 10 % foetal bovine serum (Gibco, USA) and 1 % penicillin-streptomycin solution (Gibco, USA). Experiments were performed using MSCs prior to passage 6. MSCs express a variety of stem cell-specific markers and have good proliferative and differentiation potential. The cells were tested for bacterial, fungal, mycoplasma, and viral contamination.

Exosome isolation was achieved via ultracentrifugation. Following an incubation period of 48 h in exosome-deficient medium at 37 °C, the cell culture medium was collected into 50 ml tubes, and centrifuged sequentially at 300×*g* for 10 min, 2000×*g* for 10 min, 16500×*g* for 20 min and finally 100,000×*g* for 70 min at 4 °C, with intervening PBS washes. Chitosan nanoparticles were added (1 %) and incubated at 4 °C for 10 min to generate the Chitosan Nanoparticles with exosomes (CS-E) solution. We have identified MSC-Exos, as shown in Supplementary 1 and Supplementary Fig. 2A.

2.4. Synthesis and characterization of CMCS-CEBT

For the CMCS hydrogels, 8 g of CMCS powder was dissolved in 100 ml of double-distilled water with stirring for 3 h at room temperature, culminating in the formation of hydrogels. For CMCS–CS–E, 5 ml of exosome solution (2000 μg/ml) was added to 5 ml of chitosan nanoparticles in an 8 % (w/v) solution followed by thorough mixing and incubation for 30 min at 37 °C, yielding 10 ml of CS-E solution. Subsequently, 10 ml of CS-E solution was added to 90 ml of CMCS hydrogel, resulting in the formation of CMCS–CS–E containing exosomes at a final concentration of 10 μg/ml and chitosan nanoparticles at a final concentration of 0.1 %. The CMCS-CEBT dressing was synthesized using CMCS–CS–E, BG, and TiO_2 at the designated mass ratio. Specifically, 0.1 g of BG and 0.001 g of TiO_2 were incorporated into 100 ml of CMCS–CS–E. After mixing to generate a homogenous solution, the solution was preserved at 4 °C to allow for dressing formation.

Scanning electron microscopy (SEM) was used to examine the surface features of CMCS, CMCS–CS–E, and CMCS-CEBT. Nanoparticle tracking analysis (NTA) was employed to detect the chitosan particles. To evaluate the characteristics of the materials, Fourier transform infrared (FTIR) spectroscopy was employed to assess the CMCS, CMCS–CS–E, and CMCS-CEBT. Meanwhile, the degradation characteristics of CMCS-CEBT hydrogels were explored, as shown in Supplementary 1 and Supplementary Fig. 2B.

2.4.1. Degradation characteristics of the CMCS-CEBT hydrogel

Degradation entails bulk and weight reduction of the hydrogel, with its constituents transforming into lower molecular weight entities. These fragments persistently inhabit the wound (as illustrated in Supplementary Fig. 2B).

2.5. Antibacterial activity test

The antibacterial activity of the CMCS-CEBT hydrogels against *E. coli* (a gram-negative bacterium) and *S. aureus* (a gram-positive bacterium) was determined using the bacterial counting method. After filtering and sterilizing the hydrogel with a 0.22 μm filter, administer 1 ml of each hydrogel was distributed uniformly onto a nutrient agar plate. Then, 1 ml of *E. coli* or *S. aureus* culture at a concentration of 1000 CFU/ml was added to the Petri dish of the corresponding group, and the culture was distributed evenly on the surface of the culture plate. The treated culture plate was incubated at 37 °C for 12 h. The CFUs were counted by enumerating the colonies on the agar plates and evaluating the antibacterial effect of each treatment.

2.6. Cell viability and migration

Human umbilical vein endothelial cells (HUVECs) were procured from ATTA to assess of cell proliferation and migration. HUVECs were propagated in DMEM (Gibco, USA) composed of 10 % foetal bovine serum (Gibco, USA) and 1 % penicillin streptomycin solution (Gibco, USA). For the cell viability assay, the cells were divided into three groups: the control group, CS-E (0.1 % chitosan nanoparticles containing 100 μg/ml exosomes) group and CEBT (comprising CS-E and the final concentrations of 0.1 % BG and 0.001 % TiO_2) group. Approximately 5×10^3 HUVECs cells were seeded into 96-well plates. To test the cell viability, after incubation for 24 h, 72 h and 120 h, cell counting kit (CCK-8) reagent was added and incubated for 4 h. Cell viability was measured by determining the absorbance of each well at a wavelength of 450 nm using a microplate reader. The cell proliferation experiment with the L929 cell line followed the experimental steps used for HUVECs.

Cell migration was assessed using a scratch assay as previously described. HUVECs were seeded in a 24-well culture plate at a cell density of 2×10^4 cells per well for culture. When the cells culture reached approximately 80 % confluence, a horizontal line was scratched perpendicular to the surface of the culture plate with the tip of a pipet The cells were removed after 0, 12, and 24 h, respectively, and the width of the scratch was observed under the microscope. Then, the results were subsequently analyzed.

2.7. Western blotting

Protein quantification was performed using employing a BCA assay (Thermo Fisher Scientific). Proteins (20 mg per lane) were subjected to 12 % sodium dodecyl sulfate–polyacrylamide gel electrophoresis (SDS-PAGE), and subsequently being transferred to polyvinylidene fluoride (PVDF, Immobilon-P) membranes. The membranes were blocked using TBST containing with 5 % bovine serum albumin for 1 h at room temperature, followed by an overnight incubation at 4 °C using commonly utilized antibodies: anti-VEGFA, anti-VEGFR2, anti-Calnexin, anti-TSG101, anti-CD63 and anti-CD9 antibody at a dilution of 1:500, an anti-GAPDH mouse monoclonal antibody, at a dilution of 1:10000. Subsequent iterations comprised multiple PVDF membrane rinsing steps, post which they were further incubated with secondary antibodies (an anti-rabbit or mouse antibody conjugated with horseradish peroxidase) for an extended period of 1 h at room temperature. The intensities of VEGFA, VEGFR2, Calnexin, TSG101, CD63, CD9, and GAPDH were quantified using ImageJ software.

2.8. Inflammation assay

The evaluation of both proinflammatory and anti-inflammatory mediators was conducted by utilizing a number of ELISA kits. The RAW264.7 murine macrophage line was procured from the Cell Bank of the Chinese Academy of Sciences and used in our investigation; the cells were cultured in high-glucose DMEM containing of 10 % FBS (Gibco, USA) and 1 % penicillin and streptomycin. RAW264.7 cells were propagated in 24-well plates and divided into four groups: the control (PBS) group, LPS group (lipopolysaccharide, 100 ng/mL), LPS + CS-E group (lipopolysaccharide, 100 ng/mL+ a concentration of 0.1 % chitosan nanoparticles, with 100 μg/mL exosomes) and LPS + CEBT group (lipopolysaccharide, 100 ng/mL, a blend of CS-E, 0.1%BG, and 0.001% TiO_2 nanoparticles). After a 24-h incubation duration, the resultant conditioned medium was collected for subsequent quantitation of tumour necrosis factor alpha (TNF-α), interleukin 1 beta (IL-1β), IL-6, transforming growth factor beta (TGF-β) and interleukin 10 (IL-10) concentrations by employing a the TNF-α ELISA kit, IL-1β ELISA kit, IL-6 ELISA kit, TGF-β ELISA kit and IL-10 ELISA kit, respectively; all ELISA kits were procured from suppliers such as Neobioscience and Quanticytio and used according to their respective protocols.

2.9. In vivo assay

All animal experiments in this study were approved by the research ethics committee of China-Japan Friendship Hospital (Beijing, China) and conducted in accordance with the guidelines set forth in the Guidelines for the Care and Use of Laboratory Animals of the National Institutes of Health. All mice were fed and maintained in a room with a light/dark cycle of 12 h and a stable temperature and humidity (25 °C). One series of experimental procedures were performed with male C57BL/c mice procured from SPF (China) Biotechnology Co., Ltd. that weighed between 18 and 22 g. The dorsolateral fur of these animals was removed with depilatory cream under general anaesthesia. Deep full-thickness skin defects measuring 7 mm in diameter were carefully produced utilizing dermal biopsy punches. The mice were subsequently assigned to one of three treatment groups:in the CMCS group, the wound site was treated with only CMCS hydrogel; in the CMCS–CS–E group, the wound site was treated with CMCS–CS–E hydrogel; in the CMCS-CEBT group the wound site was covered with CMCS-CEBT. The mice were maintained in an environment with a precisely regulated 12-h light/dark cycle and a consistent temperature (25 °C) and humidity. Skin repair was evaluated postoperatively on postoperative Days 3, 7, and 14 for each treatment group, with photo documentation and euthanasia via lethal injection of pentobarbital sodium as necessary.

Male db/db diabetic mice that were procured from SPF Biotechnology Co., Ltd (China), and weighed between 40 and 50 g were fed and maintained for approximately 8 weeks. The mice were divided into three groups: the CMCS group, CMCS–CS–E group and CMCS-CEBT group. A blood glucose level was higher than 16.7 mM with weight loss and polyuria was considered to indicate diabetes [26]. The diabetic wound model was established as described for the full-thickness skin injury model. Diabetic wound healing was evaluated post procedure on postoperative Days 0, 9 and 19 for both treatment modalities, with photographic evidence and euthanasia via lethal administration of pentobarbital sodium as necessary.

For evaluation of cutaneous burns, male C57 mice (weight 18–22 g) initially underwent a 10-s exposure to a thermally activated metallic alloy bar (10 mm in diameter, 51g) that was initially immersed in boiling water at a remarkably high temperature of 100 °C for 10 min prior to direct contact.

Careful decontamination of the wound site was performed under anaesthesia using iodophor on the dorsal surface for an additional 30 s on their dorsal surfaces. Postoperative photographs of the wounds were captured on Days 0, 9, and 17, and stringent wound assessment criteria were used with the animals sacrificed on Day 17 post-surgery according to the protocol.

2.10. Histological analysis

Skin tissues excised post-healing were fixed with a 10 % formalin solution, subsequently dehydrated in alcohol, and embedded in paraffin. The resultant sections (with a thickness of 5 μm) were subjected to H&E, Masson tricolour, and immunohistochemical staining protocols. Following deparaffinization, inactivation of endogenous peroxidase activity was conducted followed by an immersion in blocking solution prior to antigen retrieval. Subsequently, the sections were incubated overnight with anti-CD31, α-SMA(BM0002), as well as IL-6, IL-1β,TNF-α, and IL-10 antibodies at a temperature of 4 °C. After washing, the secondary antibody was added at 37 °C for half an hour, followed by the DAB reaction stage and subsequent hematoxylin staining. Finally, quantification of the staining intensity of CD31, α-SMA, and inflammatory factors was performed using ImageJ software to evaluate the density of blood vessels and inflammatory factor expression.

2.11. Statistical analysis

All experimental data were analyzed using the IBM SPSS Statistics 19 program and GraphPad prism 7 software. The difference between the experimental group and the control group was tested by the two-tailed unpaired student t-test, and the multi-group comparison was carried out by one-way analysis of variance (ANOVA). All data are expressed as mean ± standard deviation. $P < 0.05$ was statistically significant.

3. Results

3.1. Characterization of the CMCS-CEBT

Hydrogel pores with optimal dimensions enable the proliferation and migration of cells. They also effectively facilitate nutrient and oxygen transport [27]. Thus, we utilized scanning electron microscopy (SEM) to evaluate the pore dimensions of the composite after the incorporation of various components. As shown in Fig. 1A, the pore diameters of the three groups were as follows: 155.92 ± 17.96 μm, 153.84 ± 27.50 μm, and 162.96 ± 8.63 μm. All three groups had satisfactory pores. The range of pore dimensions for these three groups promotes the proliferation and migration of epidermal cells. The pore size of the chitosan particles was determined by nitrogen adsorption measurement analysis (NTA), as shown in Fig. 1B. The diameter of the chitosan particles was 752 ± 110 nm. Furthermore, as shown in Fig. 1C, the absorption spectra of the three groups were evaluated using Fourier transform infrared spectroscopy (FTIR), which indicated the presence of crucial hydroxyl (H)- and carboxyl (-*O*-) groups in carboxymethyl chitosan. After the addition of exosomes, BG and TiO_2, there was no change in the –OH and –COOH groups of carboxymethyl chitosan. Next, exosomes, BG and TiO2 particles adhering to the surface of carboxy were identified by SEM (Fig. 1D). Meantime, the cytotoxicity of CMCS-CEBT hydrogels was investigated, as shown in Supplementary1, Supplementary Fig. 2C and 2D.

3.2. CEBT promotes cell proliferation and migration

The progression of HUVEC and L-929 cell growth was quantified using the CCK-8 assay. In comparison to the control treatment, distinctive findings indicated that both CS-E treatment and CEBT treatment clearly stimulated the proliferation of HUVECs notably from Day 3 to Day 5, as shown in Fig. 2A. Conversely, CEBT more potently facilitated the replication of L-929 cells, surpassing the values of the CS-E group and the untreated control (Fig. 2B). Additionally, Fig. 2C shows the scratch assay for HUVECs and the semi-quantitative results for the control group, CS-E group, and CEBT group. An assessment of wound healing revealed that CEBT group displayed markedly higher migratory capacity than the other two groups, as shown in Fig. 2D. These empirical data underscore the biocompatibility advantages of the composite dressing's exosomes, bioactive glass and TiO_2 that was used in the CEBT group.

VEGF has a profound influence on vessel formation by endothelial cells. Previous studies have demonstrated that both BG and exosomes stimulate VEGFA expression [28,29]. We therefore investigated the impact of CS-E and CEBT on the expression of VEGFA and VEGFR2. As shown in Fig. 2E, CS-E and CEBT were both able to increase the expression of VEGFA and VEGFR2. Both CS-E and CEBT amplified the production of VEGFA, with CEBT causing a more notable increase (1.64 ± 0.2 vs 2.62 ± 0.49). Similarly, CS-E and CEBT boosted the production of VEGFR2, which was 1.74 ± 0.2 times and 2.42 ± 0.4 times higher than that of the control group, respectively. The overproduction of VEGFA in the CEBT group, which was consistent with the VEGFR2 expression results, promoted angiogenesis and migration in endothelial cells. Collectively, these results illustrate that CEBT notably enhanced the angiogenesis of endothelial cells by targeting VEGFA and VEGFR2.

3.3. CEBT inhibited the inflammatory response in vitro

To quantify macrophage polarization status after treatment with an

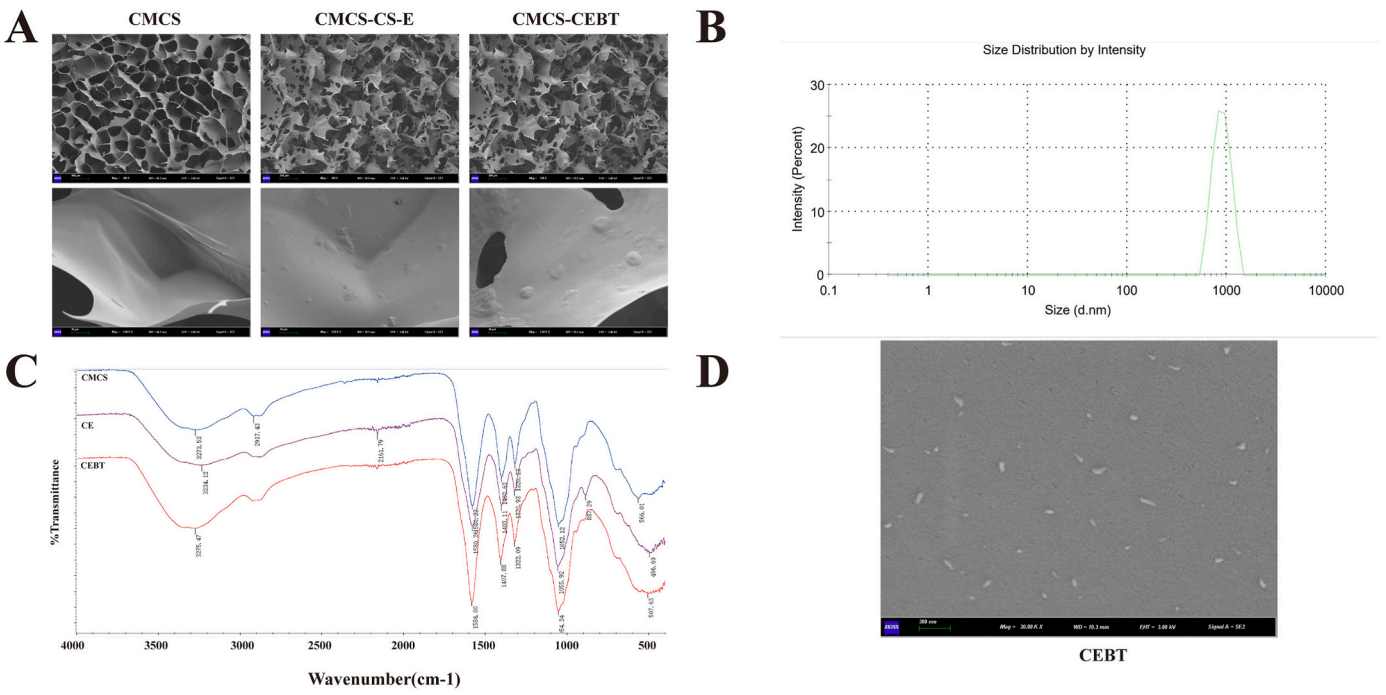

Fig. 1. Characterization of the CMCS-CEBT. A. SEM images of CMCS, CMCS–CS–E and CMCS-CEBT; B. Size distribution of CS particles; C. FTIR spectra of CMCS, CMCS–CS–E and CMCS-CEBT; D. SEM images of CMCS-CEBT.

equivalent volume of PBS (control group), LPS, LPS + CS-E, or LPS + CEBT, we evaluated the secretion of the proinflammatory factors TNF-α, IL-1β, and IL-6 by ELISA. Moreover, we evaluated the secretion of the anti-inflammatory cytokines TGF-β and IL-10 after a 24-h incubation period. By utilizing ELISA, we found that the secretion of TNF-α, IL-1β, and IL-6 in the LPS + CEBT group was notably decreased compared to that in the LPS group, and the levels of these proinflammatory mediators in the LPS + CE-E group were also markably reduced in the LPS + CE-E group compared to the LPS group (Fig. 3A, B, C). Concurrently, we observed that TGF-β and IL-10 secretion in the LPS + CS-E and LPS + CEBT groups was markedly elevated when compared to the Control and LPS groups, and the levels of these anti-inflammatory cytokines in the LPS + CEBT group were also appreciably increased when compared to those in the LPS + CS-E group (Fig. 3D and E).

3.4. Evaluation of antibacterial activity

The antibacterial potency of TiO_2 NPs markedly increases their potential for biological applications [27]. However, the concentration of TiO_2 NPs used in wound therapeutic strategies must be optimized, as excessive concentrations could induce toxicity to neural or epithelial cells. Here, we used the gram-positive bacteria *S. aureus* and gram-negative bacteria *E. coli* to evaluate the antibacterial effect of CMCS-CEBT hydrogels. As shown in Fig. 4 A and 4 B, the CMCS hydrogel exhibited weaker antibacterial activity than the CMCS-CEBT hydrogel. The CMCS-CEBT hydrogel showed stronger antibacterial activity against the gram-negative and gram-positive bacteria, including *E. coli* and *S. aureus*, respectively. The CMCS-CEBT hydrogel suppressed bacterial growth by 94.5 % ± 1.9 % for the gram -negative bacteria *E. coli*, and 92.1 % ± 1.7 % for the gram-positive bacteria *S. aureus*.

3.5. CMCS-CEBT dramatically accelerates the repair of full-thickness skin defects and significantly increases collagen deposition

To assess the efficacy of CMCS-CEBT in wound healing in vivo, we utilized the extensively employed full-thickness skin defect model. A thin film of CMCS-CEBT hydrogel residue from the final treatment remained on the wound bed, thereby effectively shielding the damaged site against extraneous environmental contaminants and diminishing the likelihood of microbial invasion. Fig. 5A shows those photographs of wounds at distinct time intervals, demonstrating a marked enhancement in the progression of skin wound repair in the CMCS-CEBT group compared with the CMCS and CMCS–CS–E groups. Notably, the majority of the wounds exhibited complete repair by Day 7 post-surgery in the CMCS-CEBT group. Fig. 5B and C shows that at each observation timepoint (Days 3, 7, and 14), the rate of wound healing in the CMCS-CEBT group was markedly higher than that in the other experimental groups, and this difference was most notable after Day 7. The gap widths of CMCS group, CMCS–CS–E group and CMCS-CEBT were 1.38 ± 0.34 mm, 2.59 ± 0.25 mm and 1.74 ± 0.25 mm, respectively. Through gap width analysis, it was found that compared with CMCS group and CMCS–CS–E group, the gap width of CMCS-CEBT was significantly smaller, as shown in Fig. 5D.

Mice were sacrificed on Day 14 post-surgery contingent upon the extent of skin wound recovery. At this timepoint, external examination indicated nearly complete healing of the skin defects of the mice in the CMCS-CEBT hydrogel treatment group. H&E staining showed that the width of the wound in the CMCS-CEBT group was the smallest amongst all the groups (Fig. 5E). The wound tissue transitioned from a granuloma stage to collagen synthesis phase within the CMCS-CEBT group, contrasting with persistent granuloma phase in the remaining control group. The subsequent seeding of collagen fibers after the onset of granulation tissue maturation greatly accelerates wound repair. Remarkably, we observed an augmented collagen deposition in the CMCS-CEBT group compared to the other groups. Masson's trichrome staining revealed the largest collagen-infiltrated area within the CMCS-CEBT group (Fig. 5F and G). Collectively, these findings suggest that CMCS-CEBT may expedite skin wound healing potentially via augmenting collagen encapsulation.

3.6. CMCS-CEBT exerts strong proangiogenic effects during the wound healing process

Evaluating the efficacy of different wound dressings requires

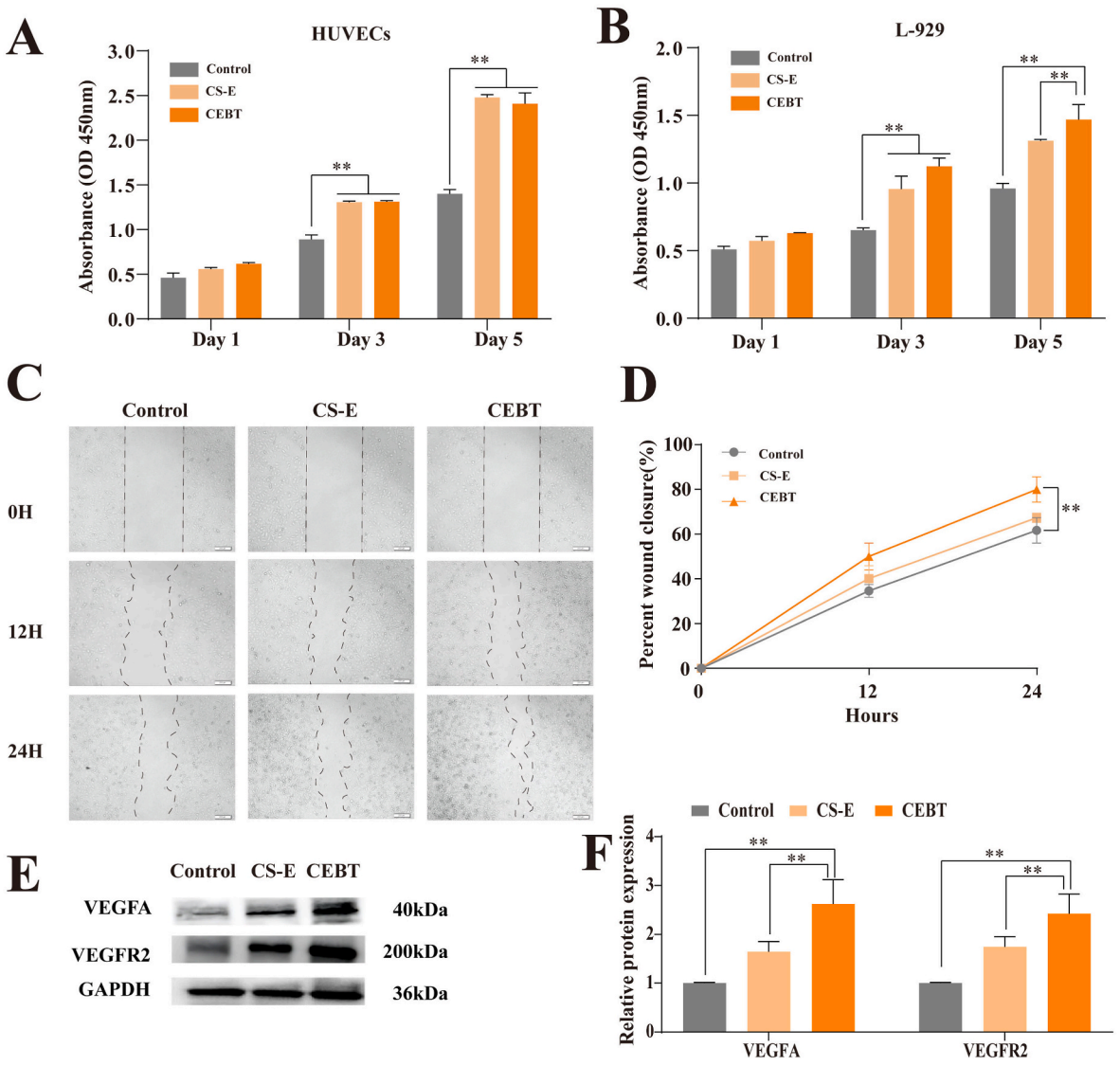

Fig. 2. CCK-8 assays of human umbilical vein endothelial cell (HUVEC) (A) and L929 (B) proliferation; C. Scratch test of HUVECs and semiquantitative analysis. D. Analyses of the wound closure. E. Western blot analysis of VEGFA and VEGFR2 protein expression in cells cocultured with CS-E and CEBT. F. Quantification of VEGFA and VEGFR2 expression. All data were normalized to GAPDH expression. Data are represented as the means ± SDs (n = 3), $^{*}P < 0.05$, $^{**}P < 0.01$.

multiple types of assessments. A crucial factor is the quantity of blood vessels present within the wound site post-healing. By employing immunohistochemical detection techniques such as CD31 and α-SMA staining, we revealed an increased density of newly formed vessels within the wound bed for the CMCS-CEBT group compared to the other groups (Fig. 6). This finding indicates that CMCS-CEBT may enhance wound healing by stimulating neovascularization. As shown in Fig. 6A and B, on the seventh day of treatment, the expression of both the α-SMA and CD31 proteins was notably higher in the wounds treated with CMCS-CEBT, suggesting that CMCS-CEBT possesses superior efficacy in initiating neovessel growth during the initial phase. Furthermore, as shown in Fig. 6C and 6 D, after 14 days, the expression of these markers remained elevated in wounds treated with the CMCS-CEBT hydrogel, underscoring the sustained angiogenic activity of the CMCS-CEBT group composite dressing. These experimental findings make a compelling case for the efficacy of the developed dressing in promoting angiogenesis.

3.7. CMCS-CEBT promotes the healing of diabetic wounds

In a subsequent study, we examined the efficacy of CMCS-CEBT in promoting the healing of diabetic skin lesions present in db/db mice. A diabetic skin injury mouse model was generated as described above. Photographs showing the evolution of these wounds over various time intervals are presented in Fig. 7A. Notably, the recovery process exhibited marked acceleration within the first nine days in the CMCS-CEBT-treated mice. By Day 19 post-surgery, the majority of these wounds had been nearly completely healed (as shown in Fig. 7B), and all animals within this cohort were euthanized at that timepoint.

H&E staining of histologic sections revealed a morphologically restored epidermis and extensive granulation tissue in the CMCS-CEBT-group (Fig. 7C). In contrast, mice from both the CMCS and CMCS–CS–E groups displayed less wound healing, along with somewhat attenuated granulation tissue development. Furthermore, Masson's trichrome staining demonstrated increased collagen fibre accumulation in the CMCS-CEBT treated mice compared to the control mice (Fig. 7D). This suggests that the ability of CMCS-CEBT to accelerate healing of diabetic skin lesions may involve the stimulation of collagen fibre formation.

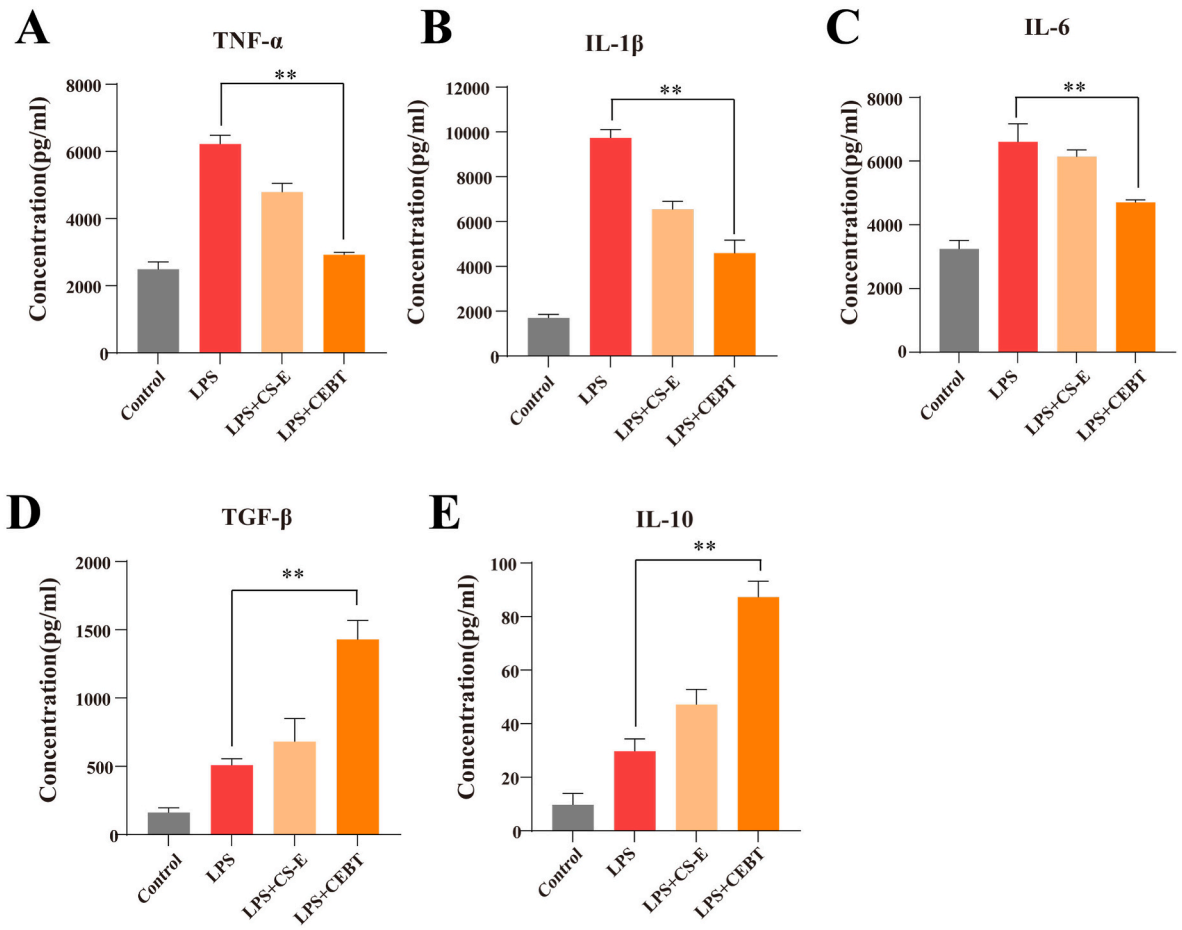

Fig. 3. Levels of TNF-α(A), IL-1β (B), IL-6 (C) and TGF-β(D), and IL-10(E) in RAW 264.7 cells treated with or without LPS, and with or without miRNA-497. Proinflammatory cytokines expression was analyzed by the enzyme-linked immunosorbent assay (ELISA). Data are the mean ± SD (n = 3). $^{*}P < 0.05$, $^{**}P < 0.01$.

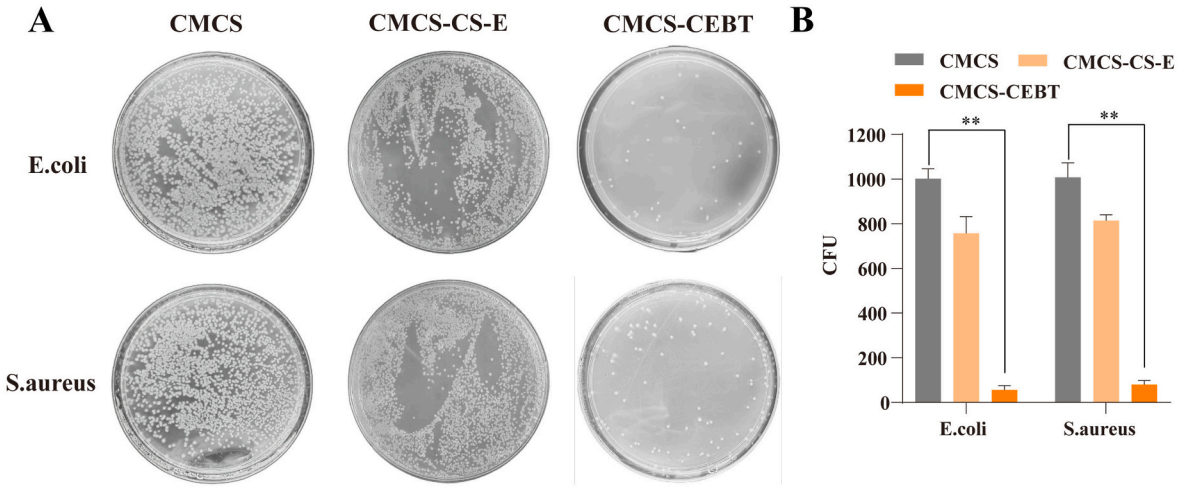

Fig. 4. Analysis of the antibacterial activity analysis of CSEB hydrogels against *E. coli* and *S. aureus*. Bacteria clones (A) and bacterial viability (B) for *E. coli* and *S. aureus* after incubation for 12 h at 37 °C. Data are the mean ± SD (n = 3). $^{*}P < 0.05$, $^{**}P < 0.01$.

3.8. CMCS-CEBT exerts strong anti-inflammatory effects during the diabetic wound healing process

As a dysregulated macrophage response has been implicated in the impaired healing of diabetic wounds, macrophages are currently being investigated as a therapeutic target for enhanced wound healing. During the diabetic wound healing process, CMCS-CEBT has considerable anti-inflammatory effects. A representative analysis of TNF-α, IL-1β and IL-6, and IL-10 levels in skin wound samples collected after various therapeutic interventions is shown in Fig. 8A. Confirmatory immunofluorescence staining of TNF-α, IL-1β, IL-6, and IL-10 underscores the strong anti-inflammatory potential of CMCS-CEBT. Notably, the TNF-α signal in the CMCS-CEBT group was much weaker than that in the CMCS and CMCS–CS–E groups (Fig. 8A and B). Additionally, the intensity of IL-1β

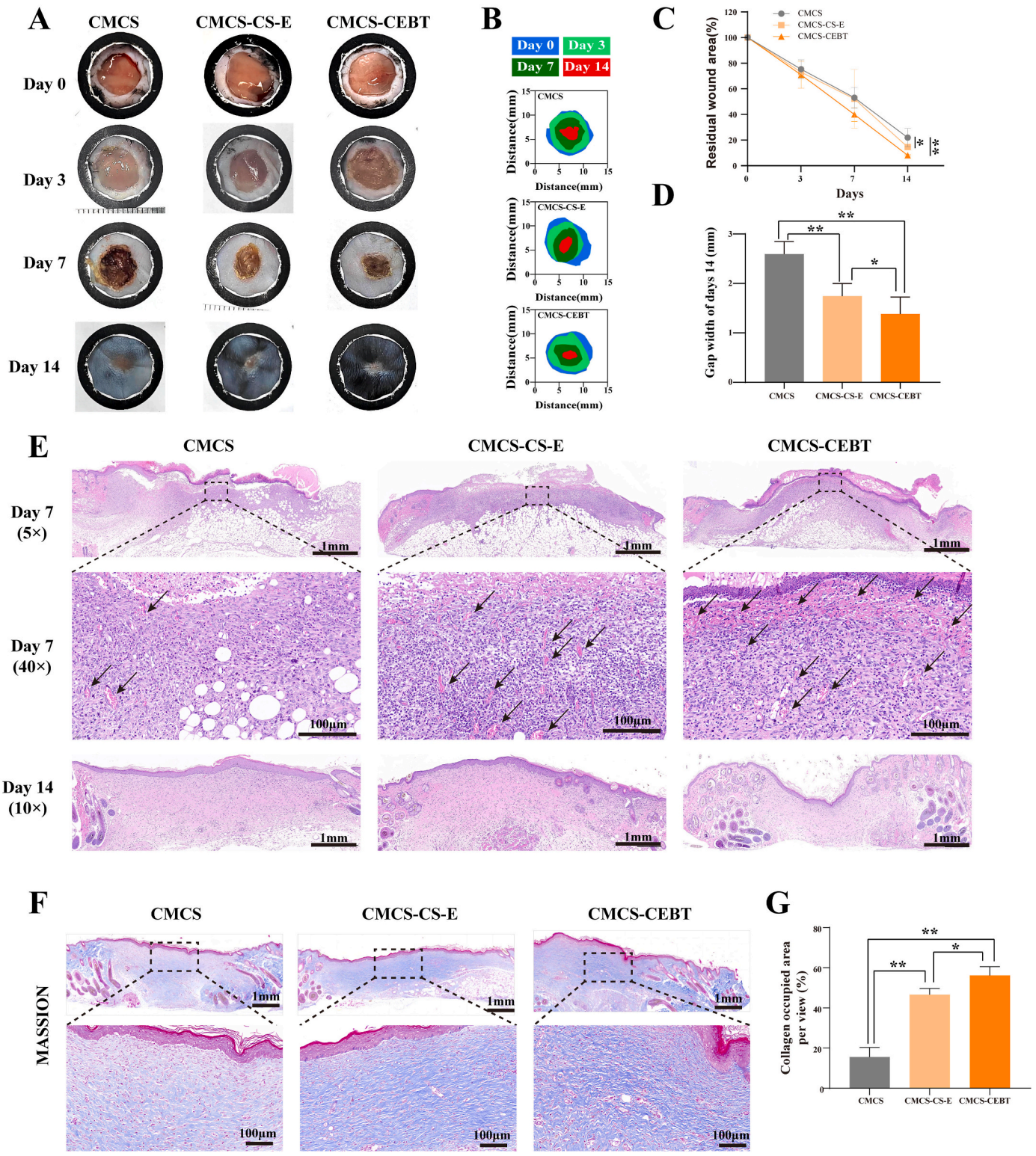

Fig. 5. A. Representative images of the wound surface in each group on days 0,3,7 and 14. B. Changes in the wound area over time; C. Analyses of the wound closure on days 0,3,7 and 14. D. Gap width on Days 14. E. H&E staining on Days 7 and 14 post-surgery, Arrows indicate angiogenesis. F. Representative images of Masson trichrome staining of the healed tissues in the wound skin defect for the CMCS hydrogel, CMCS–CS–E and CMCS-CEBT groups on Day 14 post-surgery. G. The results of statistical analysis of the relative area covered by collagen in the regenerated tissue calculated on the basis of Masson trichrome staining for each group, Data for the CMCS hydrogel group on the 14th day was set as 100 % (n = 3). *$P < 0.05$, **$P < 0.01$.

and IL-6 staining in the CMCS-CEBT collective was the lowest among all the evaluated groups. With respect to the anti-inflammatory mediator IL-10, it is worth noting that the CMCS-CEBT group displayed a significant increase in expression compared to that in the CMCS group.

4. Discussion

In this study, we engineered a combination of MSC-derived exosomes, chitosan nanoparticles, BG, TiO2 and carboxymethyl chitosan

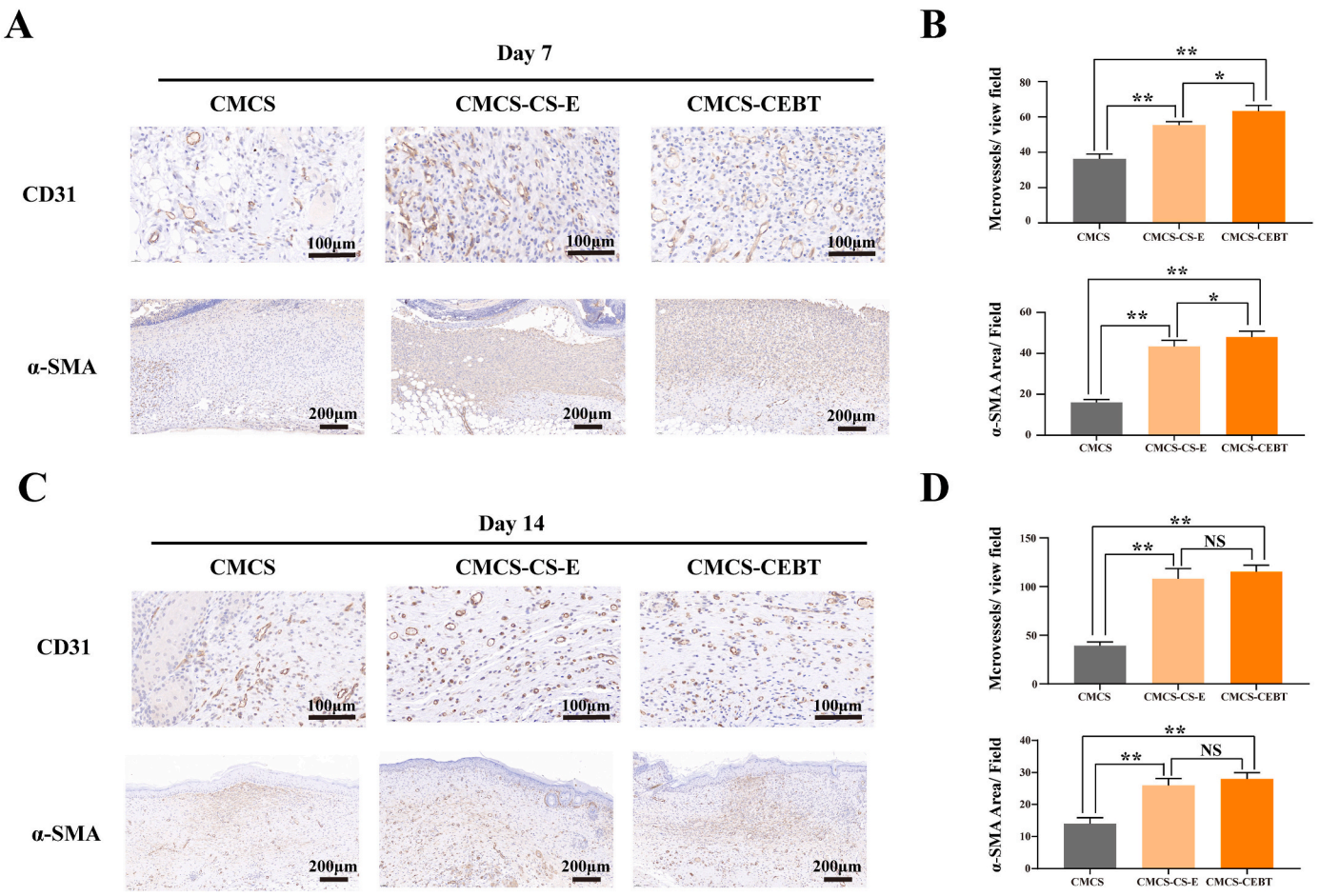

Fig. 6. The effect of hydrogels on angiogenesis in the full-thickness defect of mouse models. Representative photos of CD31 immunohistochemical staining. A) on Day 7. B) and on Day 14 post-surgery. The expression of the protein CD31 is shown in a brown, while blue dots indicated the cell nuclei. $^{*}P < 0.05$, $^{**}P < 0.01$, NS═No statistical significance.

hydrogel composites (CMCS-CEBT) which was employed in three distinct skin wound models: full-thickness injury model, a diabetic injury model and a burn wound model. The primary goal was to validate the potential of CMCS-CEBT to stimulate cell migration, encourage neovascularization, exert an anti-inflammatory effects and exhibit integrated antimicrobial activity in vitro. Our results demonstrated that CMCS-CEBT is remarkably effective in enhancing the healing process for full-thickness injuries, diabetic skin defects, and burn wounds. For instance, CEBT was found to stimulate the biological activity of HUVECs and L929 cells, with increases in proliferation and migration, and even to facilitate in vitro wound repair. These findings indicate that CMCS-CEBT accelerates wound healing by virtue of its anti-inflammatory properties and its ability to stimulate angiogenesis and collagen deposition. This represents a promising strategy for improving the healing trajectory of acute and chronic diabetic wounds and burn wounds.

Numerous studies have suggested that exosomes derived from MSCs contain mRNA, miRNA, growth factors and diverse proteins and thereby playing integral roles in numerous physiological processes such as haemostasis and thrombosis; inflammation; immune interaction; angiogenesis; and wound healing processes such as re-epithelialization, new vessel formation/vascular maturation, collagen deposition, and differentiation of hair follicles and sebaceous gland development [30–33]. However, despite their immense potential in the clinical setting, the rapid swelling and inactivation of exosomes at room temperature prohibit their practical application. The binding of chitosan nanoparticles to exosomes can serve as a protective shield against their destructive conditions, slowing exosome degradation and thereby protecting the exosomes [20,34]. Our experimental data indicated that CS-E and CEBT demonstrated good healing promoting effects in both cellular experiments and animal trials.

BG exhibits immense potential for skin repair due to its substantial biological activity [34]. During the early stages of wound healing, BG mitigates inflammatory responses, promoting epithelial cell and fibroblast migration and thereby expediting re-epithelialization at the wound site [35,36]. Moreover, BG induces angiogenesis; in later stages, it aids in attenuating skin scar formation, thereby promoting the growth of nascent epidermal tissue. Nevertheless, the inherent brittleness of BG impedes its application during skin wound healing. Combining of polymer hydrogels and nanoscale BG represents a feasible solutions for this problem and this approach can be adjusted to modulate inflammation at the skin wound site. Hybrid materials constructed from hydrogels and BG can optimize leverage their therapeutic effects while synergistically accelerating skin wound repair [37].

TiO_2 is an extensively utilized nanoparticle, and its photocatalytic and antibacterial properties have been verified. Titanium-coated wound dressings can significantly enhance wound healing efficiency [38,39]. Further research has shown that the combination of TiO2 with various nanoparticles amplifies its potency and efficacy. TiO_2 can easily penetrate the interstitial structure of the cell wall and enter the cytoplasm to disrupt the standard metabolism in bacterial cells, or directly interact with the phosphate groups in DNA to suppress the proliferation of bacteria, particularly for the gram-negative bacteria [40]. This study confirmed the antibacterial effects of TiO2 NPs on the bacteria *E. coli* and *S. aureus* bacteria. Cell experiments verified that the effects of CEBT

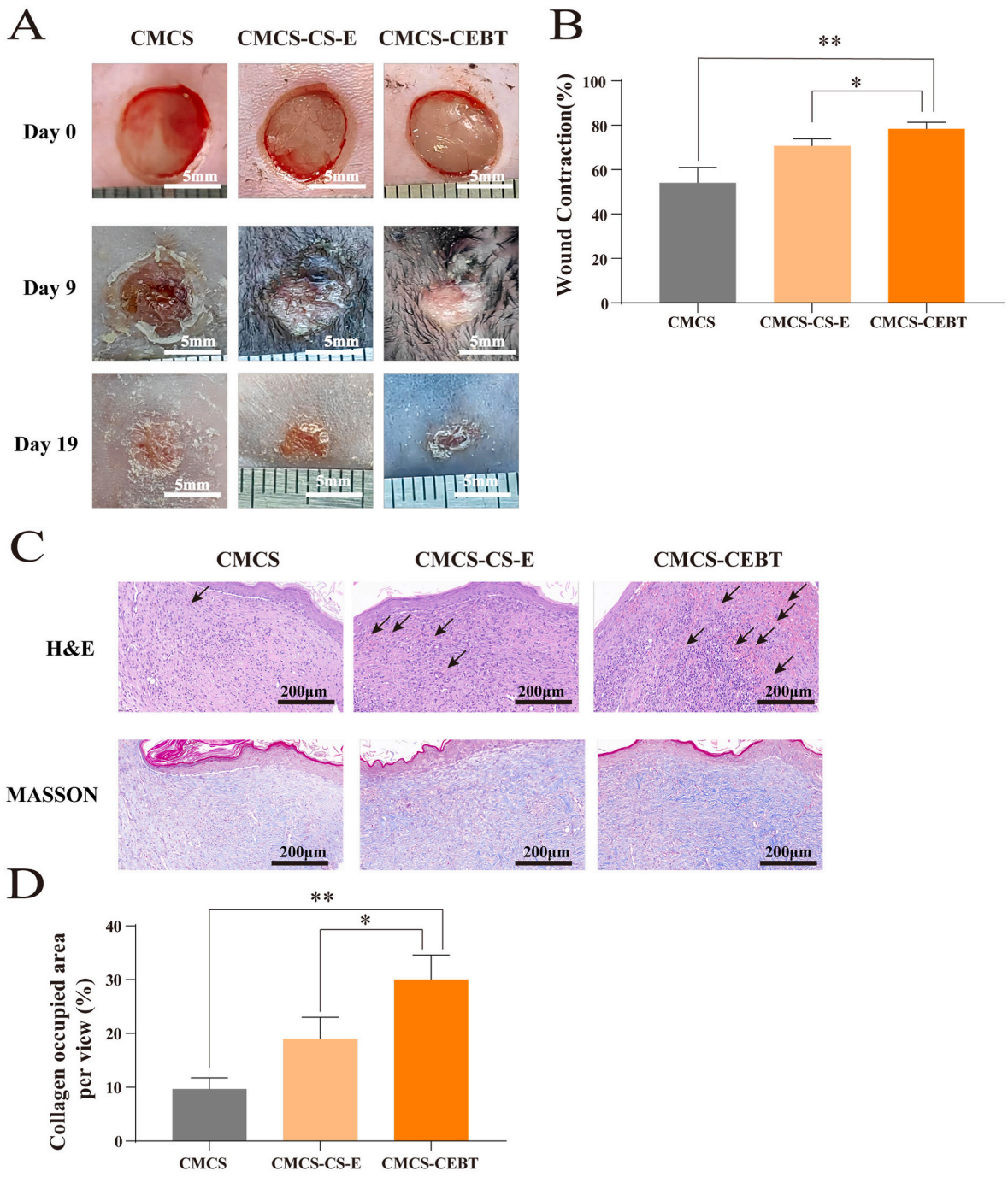

Fig. 7. The effect of hydrogels on angiogenesis in the full-thickness defect of DB mice models. A. Representative images of the wound surface in each group on Days 0,9 and 19 post-surgery. B. Changes in the wound area over time. C. H&E and Massion staining on Days 19 post-surgery, Arrows indicate angiogenesis. D. The results of statistical analysis of the relative area covered by collagen in the regenerated tissue on the basis of Masson staining for each group, Data for the CMCS hydrogel group on Day 19 post-surgery was set as 100 % (n = 3). *$P < 0.05$, **$P < 0.01$.

on the viability and activity of HUVECs and L-929 cells are comparable to those of CE-S. Nonetheless, the outcomes of the antimicrobial activity experiment underscored that CEBT outperforms CS-E, signifying its superior antibacterial effect. Hence, we posit that the incorporation of TiO2 enhances the antibacterial capacity of the composite material without substantially affecting cellular viability.

Presently, there is a need for a method involving MSC-exosomes and BG to be validated for the treatment and repair of both acute and chronic wounds. Previous studies suggest that CMCS can encapsulate exosomes, achieving a high survival rate and biological activity of MSC-exosomes within the material [41]. Implantation of allogeneic MSC-Exos encapsulated by CMCS into diabetic wounds in rats demonstrated efficacious acceleration of the wound healing rate and increases in the proliferation of granulation tissue cells and angiogenesis. Consequently, to augment wound-healing performance through the combination of hydrogels with bioactive substances, we elected to treat acute and chronic wounds using MSC-exosomes coupled with CMCS. We synthesized a compound composed of MSC-exosomes, chitosan nanoparticles, BG, and TiO2 to sustain the biological activity of exosomes and provide sustained release of exosomes and other active components at the wound site to facilitate wound healing. To our knowledge, this is the first study to investigate the efficacy of CMCS hydrogel-encapsulated

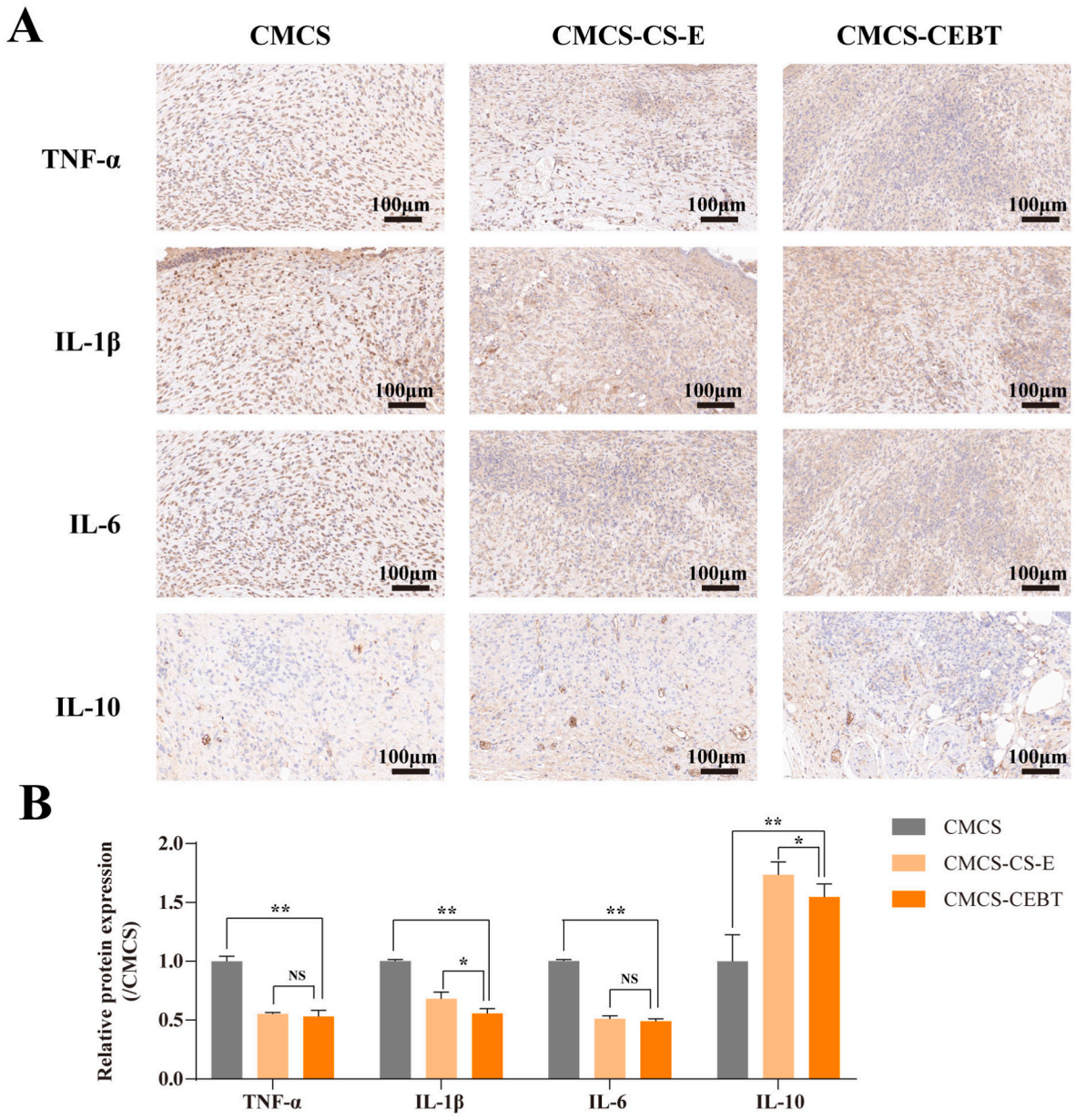

Fig. 8. A. Representative photos of TNF-α, IL-1β, IL-6 and IL-10 immunohistochemical staining on Day 19 after wound establishment. B. Analysis of relative proinflammatory cytokine and anti-inflammatory cytokine expression. Data for the CMCS hydrogel group on Day 19 post-surgery were set as 100 % (n = 3). $^{*}P < 0.05$, $^{**}P < 0.01$, NS═No statistical significance.

MSC-exosomes combined with BG and TiO2 in facilitating wound healing in both acute and chronic diabetic wounds.

Wound healing is an intricate process that involves various cell types, such as keratinocytes, endothelial cells, fibroblasts, platelets, and macrophages, in addition to diverse biochemical factors produced by these cells [42] The impairment of angiogenesis is an important factor delaying wound healing progression in chronic diabetic wounds. This study validated the efficacy of CEBT in promoting healing through three types of wound models. In the acute skin injury model, a significant increase in healing was observed on Day 7 post-injury in the CMCS-CEBT group. Notably, at this timepoint, both the number of blood vessels and collagen deposition within the regrowing tissue were notably higher in the CMCS-CEBT group than in the control group and CS-E group. To elucidate the mechanisms underlying the observed effect on wound healing, we performed CD31 and α-SMA immunohistochemistry on Day 14 in a full-thickness skin wound model and quantified the microvessel density (MVD) at the lesion site. The data suggested that both the CMCS–CS–E and CMCS-CEBT treatments promoted angiogenesis; additionally, compared with that of the CMCS–CS–E group, the propensity for angiogenesis was increased significantly in the CMCS-CEBT group, demonstrating the likely retention and sustained release of additional bioactive compounds from functional BG after application of the hydrogel to the skin wound. In vitro, we noted that CEBT promoted the proliferation and migration of HUVECs more potently than CS-E. Angiogenesis typically begins with endothelial cell proliferation prior to migration, attachment, and differentiation. Proliferation and migration are thus fundamental processes for angiogenesis, which markedly increased in the CEBT group. This finding implies that the persistent release of biologically active substances from the composite material may promote angiogenesis via expedited endothelial cell proliferation and migration.

Repair of the human skin barrier is divided into four sequential phases: haemostasis, inflammation, hyperplasia, and reconstruction. All of these phases are intertwined, and excessive prolongation of

inflammation adversely impacts subsequent regeneration. Hyper-inflammation and vascular complications resulting from elevated glucose levels around diabetic wounds extend the inflammatory phase, thereby decelerating the wound healing course [43]. Mirza et al.'s research indicated increased IL-1β levels in diabetic wound tissues. Delayed wound healing substantially increases the risk of wound infection, leading to the need for surgical debridement and further disrupting the vasculature surrounding the wound, which impairs the healing process and establishes a vicious cycle. Previous studies revealed that direct inhibition of the IL-1β pathway induces macrophage conversion from an inflamed phenotype to a reparative phenotype, facilitating accelerated wound healing in mice [44,45]. According to our study results, CMCS-CEBT reduces the expression of inflammatory factors (TNF-α, IL-1β and IL-6), increases the expression of anti-inflammatory factors (IL-10), and promotes neovascularization and collagen deposition, thereby exerting a restorative influence on diabetic wound healing. Similarly, in the burn wound model, CMCS-CEBT increased epidermal thickness and collagen deposition, with superior outcomes compared to CMCS and CMCS–CS–E, as illustrated in Supplementary Fig. 3.

The novelty and clinical significance of this study are as follows: CMCS–CS–E and CMCS-CEBT treatment resulted in a reduced wound area at 7–9 days post-treatment in the three models. In addition, CMCS-CEBT induced an accelerated healing rate compared with that of the other treatment groups. Presumably, MSC-exosomes play a significant role in the initial phase of wound repair. Nevertheless, due to their susceptibility to inactivation in extracellular environments, CMSC-exosomes fail to sustainably demonstrate efficacy during the later stages of wound healing. In the CMCS-CEBT group, the bioactivity of the biomaterial was preserved in the presence of BG, leading us to speculate that this combination of organic and inorganic active substances resulted in increased, ongoing, and rapid wound healing, for both acute and chronic wounds.

There are several limitations of this study. First, the study failed to elucidate the specific molecular mechanisms underlying angiogenesis after intravenous transplantation of CMCS-CEBT. While CEBT proved effective in augmenting VEGF and VEGFR expression in HUVECs in vitro, data regarding the expression patterns of downstream proteins and in vivo experiments are needed. In addition, further research is needed to delineate the mechanism by which BG and exosomes interact to regulate angiogenesis. Second, individual release profiles of the active components—exosomes and BG—in the composite material were not examined in this study. This gap should be addressed in future studies. Third, we failed to optimize the concentrations of the components of the composite dressing, even though we observed promising wound-healing outcomes. A more effective dose or ratio of components may exist, and the concentrations of the included components should thus be optimized.

5. Conclusion

In conclusion, the developed compound shows a strong ability to promote the recovery of acute and chronic skin wounds. In this study, the combination of exosomes and BG acted on the wound tissue continuously over time, enhancing vascularization of granulation tissues and collagen deposition, culminating in the rapid resolution of both acute and chronic diabetic wounds as well as burn wounds. The carboxymethyl chitosan hydrogel degrades rapidly upon administration. It can regulate the release of a variety of biochemical compounds, serving as an ideal bioscaffold that is suitable for the intricate environment of acute and chronic diabetic wounds.

Declaration of competing interest

The authors declare no conflict of interest.

Conflicts of interest

All authors declare no conflicts of interest.

CRediT authorship contribution statement

Shunlai Shang: Writing – original draft, Supervision, Software, Project administration, Investigation, Funding acquisition, Data curation, Conceptualization. **Kaiting Zhuang:** Supervision, Software, Project administration, Investigation, Data curation. **Jianwen Chen:** Validation, Software, Investigation, Data curation. **Ming Zhang:** Supervision, Investigation, Funding acquisition, Conceptualization. **Shimin Jiang:** Writing – original draft, Software, Resources, Project administration, Formal analysis, Conceptualization. **Wenge Li:** Writing – review & editing, Visualization, Software, Project administration, Investigation, Funding acquisition, Data curation, Conceptualization.

Acknowledgements

This work was supported by National High Level Hospital Clinical Research Funding, (2023-NHLHCRF-YS-01), Elite Medical Professionals Project of China-Japan Friendship Hospital (ZRJY2023-GG06), the China Postdoctoral Science Foundation (Certificate Number: 2023M733986 and 2023T160741), Cross-sectional project of China-Japan Friendship Hospital(Certificate Number:2023-HX-JC-10), International Association of Chinese Nephrologists Research Grant(No. IACNRG-01) and Beijing Hospitals Authority Clinical medicine Development of special funding support(Certificate Number: ZLRK202308).

Appendix B. Supplementary data

Supplementary data to this article can be found online at https://doi.org/10.1016/j.bioactmat.2023.12.026.

References

[1] A. Nourian Dehkordi, et al., Skin tissue engineering: wound healing based on stem-cell-based therapeutic strategies, Stem Cell Res. Ther. 10 (1) (2019) 111.
[2] C. Dai, S. Shih, A. Khachemoune, Skin substitutes for acute and chronic wound healing: an updated review, J. Dermatol. Treat. 31 (6) (2020 Sep) 639–648.
[3] F. Rangatchew, P. Vester-Glowinski, B.S. Rasmussen, E. Haastrup, L. Munthe-Fog, M.L. Talman, C. Bonde, K.T. Drzewiecki, A. Fischer-Nielsen, R. Holmgaard, Mesenchymal stem cell therapy of acute thermal burns: a systematic review of the effect on inflammation and wound healing, Burns 47 (2) (2021 Mar) 270–294.
[4] R.T. Chitturi, et al., The role of myofibroblasts in wound healing, contraction and its clinical implications in cleft palate repair, J. Int. Oral Health 7 (3) (2015) 75–80.
[5] C. Dai, S. Shih, A. Khachemoune, Skin substitutes for acute and chronic wound healing: an updated review, J. Dermatol. Treat. 31 (6) (2020) 639–648.
[6] P. Goodarzi, et al., Tissue engineered skin substitutes, Adv. Exp. Med. Biol. 1107 (2018) 143–188.
[7] J. Holl, et al., Chronic diabetic wounds and their treatment with skin substitutes, Cells 10 (3) (2021).
[8] W. Chen, et al., Simple and fast isolation of circulating exosomes with a chitosan modified shuttle flow microchip for breast cancer diagnosis, Lab Chip 21 (9) (2021) 1759–1770.
[9] A. Kumar, et al., The polysaccharide chitosan facilitates the isolation of small extracellular vesicles from multiple biofluids, J. Extracell. Vesicles 10 (11) (2021) e12138.
[10] N. Kosaric, H. Kiwanuka, G.C. Gurtner, Stem cell therapies for wound healing, Expet Opin. Biol. Ther. 19 (6) (2019) 575–585.
[11] Z. Azari, et al., Stem cell-mediated angiogenesis in skin tissue engineering and wound healing, Wound Repair Regen. 30 (4) (2022) 421–435.
[12] X. Qiu, et al., Exosomes released from educated mesenchymal stem cells accelerate cutaneous wound healing via promoting angiogenesis, Cell Prolif. 53 (8) (2020) e12830.
[13] L. Teng, et al., Exosomes derived from human umbilical cord mesenchymal stem cells accelerate diabetic wound healing via promoting M2 macrophage polarization, angiogenesis, and collagen deposition, Int. J. Mol. Sci. 23 (18) (2022).
[14] D. Bian, et al., The application of mesenchymal stromal cells (MSCs) and their derivative exosome in skin wound healing: a comprehensive review, Stem Cell Res. Ther. 13 (1) (2022) 24.
[15] R. Huang, et al., Recent advances in nanotherapeutics for the treatment of burn wounds, Burns Trauma 9 (2021) tkab026.
[16] W. Wang, et al., Nano-drug delivery systems in wound treatment and skin regeneration, J. Nanobiotechnol. 17 (1) (2019) 82.

[17] Y. Chen, et al., Magnesium oxide nanoparticle coordinated phosphate-functionalized chitosan injectable hydrogel for osteogenesis and angiogenesis in bone regeneration, ACS Appl. Mater. Interfaces 14 (6) (2022) 7592–7608.
[18] Q. Bai, et al., Potential applications of nanomaterials and technology for diabetic wound healing, Int. J. Nanomed. 15 (2020) 9717–9743.
[19] B.R. Rizeq, et al., Synthesis, bioapplications, and toxicity evaluation of chitosan-based nanoparticles, Int. J. Mol. Sci. 20 (22) (2019).
[20] P.K. Raghav, et al., Mesenchymal stem cell-based nanoparticles and scaffolds in regenerative medicine, Eur. J. Pharmacol. 918 (2022) 174657.
[21] S. Kargozar, S. Hamzehlou, F. Baino, Can bioactive glasses be useful to accelerate the healing of epithelial tissues? Mater. Sci. Eng., C 97 (2019) 1009–1020.
[22] E. Zeimaran, et al., Advances in bioactive glass-containing injectable hydrogel biomaterials for tissue regeneration, Acta Biomater. 136 (2021) 1–36.
[23] Z. Shariatinia, Carboxymethyl chitosan: properties and biomedical applications, Int. J. Biol. Macromol. 120 (Pt B) (2018) 1406–1419.
[24] J. Holl, C. Kowalewski, Z. Zimek, P. Fiedor, A. Kaminski, T. Oldak, M. Moniuszko, A. Eljaszewicz, Chronic diabetic wounds and their treatment with skin substitutes, Cells 10 (3) (2021 Mar 15) 655.
[25] A. Shpichka, D. Butnaru, E.A. Bezrukov, R.B. Sukhanov, A. Atala, V. Burdukovskii, Y. Zhang, P. Timashev, Skin tissue regeneration for burn injury, Stem Cell Res. Ther. 10 (1) (2019 Mar 15) 94.
[26] M. Wang, C. Wang, M. Chen, Y. Xi, W. Cheng, C. Mao, T. Xu, X. Zhang, C. Lin, W. Gao, Y. Guo, B. Lei, Efficient angiogenesis-based diabetic wound healing/skin reconstruction through bioactive antibacterial adhesive ultraviolet shielding nanodressing with exosome release, ACS Nano 13 (9) (2019 Sep 24) 10279–10293, https://doi.org/10.1021/acsnano.9b03656.
[27] B. Li, et al., Synthesis, characterization, and antibacterial activity of chitosan/TiO2 nanocomposite against Xanthomonas oryzae pv. oryzae, Carbohydr. Polym. 152 (2016) 825–831.
[28] A.G.S. de Laia, et al., Cobalt-containing bioactive glass mimics vascular endothelial growth factor A and hypoxia inducible factor 1 function, J. Biomed. Mater. Res. 109 (7) (2021) 1051–1064.
[29] X. Li, et al., Magnetic targeting enhances the cutaneous wound healing effects of human mesenchymal stem cell-derived iron oxide exosomes, J. Nanobiotechnol. 18 (1) (2020) 113.
[30] A. Shpichka, et al., Skin tissue regeneration for burn injury, Stem Cell Res. Ther. 10 (1) (2019) 94.
[31] N.B. Vu, et al., Stem cell-derived exosomes for wound healing: current status and promising directions, Minerva Med. 112 (3) (2021) 384–400.
[32] Y. An, et al., Exosomes from adipose-derived stem cells and application to skin wound healing, Cell Prolif. 54 (3) (2021) e12993.
[33] C. Zhou, et al., Stem cell-derived exosomes: emerging therapeutic opportunities for wound healing, Stem Cell Res. Ther. 14 (1) (2023) 107.
[34] Y. Ju, et al., Extracellular vesicle-loaded hydrogels for tissue repair and regeneration, Mater Today Bio 18 (2023) 100522.
[35] T.H. Kim, et al., Anti-inflammatory actions of folate-functionalized bioactive ion-releasing nanoparticles imply drug-free nanotherapy of inflamed tissues, Biomaterials 207 (2019) 23–38.
[36] F. Tang, et al., Bioactive glass promotes the barrier functional behaviors of keratinocytes and improves the Re-epithelialization in wound healing in diabetic rats, Bioact. Mater. 6 (10) (2021) 3496–3506.
[37] Y. Zhu, et al., Modulation of macrophages by bioactive glass/sodium alginate hydrogel is crucial in skin regeneration enhancement, Biomaterials 256 (2020) 120216.
[38] D. Archana, et al., In vivo evaluation of chitosan-PVP-titanium dioxide nanocomposite as wound dressing material, Carbohydr. Polym. 95 (1) (2013) 530–539.
[39] H. Motasadizadeh, et al., Development of PVA/Chitosan-g-Poly (N-vinyl imidazole)/TiO(2)/curcumin nanofibers as high-performance wound dressing, Carbohydr. Polym. 296 (2022) 119956.
[40] N.A. Ismail, et al., Gellan gum incorporating titanium dioxide nanoparticles biofilm as wound dressing: physicochemical, mechanical, antibacterial properties and wound healing studies, Mater. Sci. Eng., C 103 (2019) 109770.
[41] X. Geng, et al., A multifunctional antibacterial and self-healing hydrogel laden with bone marrow mesenchymal stem cell-derived exosomes for accelerating diabetic wound healing, Biomater. Adv. 133 (2022) 112613.
[42] S. Werner, R. Grose, Regulation of wound healing by growth factors and cytokines, Physiol. Rev. 83 (3) (2003) 835–870.
[43] M. Sharifiaghdam, et al., Macrophages as a therapeutic target to promote diabetic wound healing, Mol. Ther. 30 (9) (2022) 2891–2908.
[44] C. Tu, et al., Promoting the healing of infected diabetic wound by an anti-bacterial and nano-enzyme-containing hydrogel with inflammation-suppressing, ROS-scavenging, oxygen and nitric oxide-generating properties, Biomaterials 286 (2022) 121597.
[45] X. Zeng, et al., Chitosan@Puerarin hydrogel for accelerated wound healing in diabetic subjects by miR-29ab1 mediated inflammatory axis suppression, Bioact. Mater. 19 (2023) 653–665.